Journal of Earthquake Engineering, Vol 12, Iss 4, pp 534-554, 2008
ISSN: 1363-2469 print / 1559-808X online
DOI: 10.1080/13632460701673076

VECTOR-VALUED INTENSITY MEASURES INCORPORATING SPECTRAL SHAPE FOR PREDICTION OF STRUCTURAL RESPONSE

JACK W. BAKER* **and C. ALLIN CORNELL**
Dept. of Civil and Environmental Engineering, Stanford University
Stanford, California 94305, USA

Received 15 September, 2006
Accepted 28 August, 2007

Vector-valued ground motion intensity measures (*IM*s) are developed and considered for efficiently predicting structural response. The primary *IM* considered consists of spectral acceleration at the first-mode structural period along with a measure of spectral shape which indicates the spectral acceleration value at a second period. For the *IM* to effectively predict response, this second period must be selected intelligently in order to capture the most relevant spectral shape properties. Two methods for identifying effective periods are proposed and used to investigate *IM*s for example structures, and an improvement in the efficiency of structural response predictions is shown. A method is presented for predicting the probability distribution of structural response using a vector *IM* while accounting for the effect of collapses. The ground motion parameter ε is also considered as part of a three-parameter vector. It is seen that although the spectral shape parameter increases the efficiency of response predictions, it does not fully account for the effect of ε. Thus, ε should still be accounted for in response prediction, either through informed record selection or by including ε in the vector of *IM* parameters.

Keywords: intensity measure (*IM*); spectral shape; dynamic analysis; ground motion hazard; epsilon (ε).

1. Introduction

When assessing response of a structure using dynamic analysis, it is important to identify ground motion properties that are related to the resulting structural response. These properties are often referred to as ground motion intensity measures, or *IM*s. Intensity measures known to relate to response of nonlinear multi-degree-of-freedom structures include elastic response spectral values (i.e., response of elastic single-degree-of-freedom structures) and spectral shape, which measures the relative energy in a ground motion at multiple periods. In this paper, consideration is given to vector-valued intensity measures

* Stanford University
Stanford, CA 94305-4020, USA
Phone: +1 650 725 2573
E-mail: bakerjw@stanford.edu

consisting of spectral acceleration at the first-mode period of the structure, $Sa(T_1)$, plus a measure of spectral shape. Vectors of three parameters will also be considered briefly. Intuitively, these vectors contain more information about the ground motion than $Sa(T_1)$ alone and should thus be more effective at predicting the response of a structure. This will be confirmed, and criteria for finding an optimal set of *IM* parameters will be described.

In addition to making response predictions as a function of this vector of parameters, probabilistic seismic hazard analysis can be used to calculate the rates of occurrence of ground motions with a range of ground motion intensities. The rates of occurrence of ground motions can then be coupled with associated structural response predictions to compute the annual frequency of exceeding a given level of structural response. An example of this procedure is seen in the work of the Pacific Earthquake Engineering Research (PEER) Center [Cornell and Krawinkler 2000]. Here, the response of a structure is termed an Engineering Demand Parameter, or *EDP*. The annual frequency of exceeding a given *EDP* is calculated as

$$\lambda_{EDP}(z) = \sum_{\text{all } x_i} P(EDP > z \mid IM = x_i) \cdot \Delta\lambda_{IM}(x_i) \tag{1.1}$$

where $\lambda_{EDP}(z)$ is the annual frequency of exceeding a given *EDP* value z, $\lambda_{IM}(x_i)$ is the annual frequency of exceeding a given *IM* value x_i (commonly referred to as a ground motion hazard curve), and $\Delta\lambda_{IM}(x_i) = \lambda_{IM}(x_i) - \lambda_{IM}(x_{i+1})$ is approximately the annual frequency of $IM = x_i$. The final element of this equation is $P(EDP > z|IM = x_i)$, the probability of exceeding a specified *EDP* level, given a level of *IM*. The result from Eq. (1.1) is important because it directly indicates the safety of a structure in terms of response levels. Performance-based engineering assessments proposed by the PEER Center are based on this calculation. To make this structural response prediction more efficiently using a vector *IM*, the calculation must be generalized as discussed below.

Given that $Sa(T_1)$ has been verified as a useful predictor of structural response for a wide class of structures [e.g., Shome *et al.* 1998], it will be incorporated here in all considered vectors. The parameter $R_{T1,T2} = Sa(T_2) / Sa(T_1)$ will be used to measure spectral shape. This parameter, illustrated in Figure 1, has also been found by others to be a useful predictor of structural response [Cordova *et al.* 2001, Vamvatsikos and Cornell 2005]. Together, $Sa(T_1)$ and $R_{T1,T2}$ define two points on a ground motion's response spectrum. A range of possible T_1 values were considered, and the first-mode elastic period of the structure was seen to be an effective choice for most considered cases. Therefore, T_1 will be fixed at the first-mode structural period, with T_2 then chosen to effectively predict the response of the structure.

Choice of T_2 for a given analysis situation will be discussed, using two complementary criteria. A method for prediction of structural response using a vector *IM* is also developed for use here and for more general applications. Vectors consisting of three parameters will also be considered, in order to determine whether further addition of *IM* parameters results in additional prediction efficiency gains. The ground motion parameter ε, seen to be an effective *IM* parameter in previous work [Baker and Cornell

2005a], is considered to determine whether it accounts for spectral shape in a manner similar to $R_{T1,T2}$.

2. Prediction of Structural Response Using a Scalar IM

A method is presented here for obtaining the structural response prediction $P(EDP>z|IM=x_i)$ used in (1.1). The method will be generalized later for use with vector *IM*s. The method used here requires a suite of earthquake records, all at the same *IM* value $Sa(T_1)=x$; in this study, 40 records are used at each *IM* level. The target $Sa(T_1)$ level is obtained by scaling the amplitudes of a suite of historical earthquake records so that they have the appropriate $Sa(T_1)$ value [e.g., Shome et al. 1998]. Here the same records are used for all $Sa(T_1)$ levels, although one can use different records at various levels if probabilistic seismic hazard analysis (PSHA) disaggregation suggested that important record properties were changing [Baker and Cornell 2006a]. The suite of *n* records is used to perform nonlinear dynamic analysis on a model of the structure, resulting in *n* corresponding values of *EDP*. Because *EDP* values vary from record to record, *EDP* given $Sa(T_1)=x$ can be modeled as a random variable with an unknown distribution, with *n* samples from the distribution obtained from dynamic analysis. The distribution must then be estimated from these samples in order to calculate the probability that *EDP* will be greater than a given value at the specified $Sa(T_1)$ level.

The distribution of responses, accounting for collapses, is obtained using the method of Shome and Cornell [2000]. The records causing collapse at the given $Sa(T_1)$ level (as indicated by extreme deformations causing non-convergence of the dynamic analysis algorithm), are used to estimate the probability of collapse, denoted *C*

$$P\left(C \mid Sa(T_1)=x\right)=\frac{\text{number of records causing collapse}}{\text{total number of records}} \tag{2.1}$$

The remaining non-collapse responses have been found to be well represented by a lognormal distribution, at least for the maximum interstory drift ratio response parameter considered here [Shome 1999, Aslani and Miranda 2003]. Thus the natural logarithm of *EDP* is normally distributed, and the parameters for this distribution can be estimated using the method of moments [Benjamin and Cornell 1970]. The probability that *EDP* exceeds *z* given $Sa(T_1) = x$ is

$$P\left(EDP>z \mid Sa(T_1)=x,\overline{C}\right)=1-\Phi\left(\frac{\ln z-\hat{\mu}_{\ln EDP|Sa(T_1)=x}}{\hat{\beta}_{\ln EDP|Sa(T_1)=x}}\right) \tag{2.2}$$

where $\hat{\mu}_{\ln EDP|Sa(T_1)=x}$ and $\hat{\beta}_{\ln EDP|Sa(T_1)=x}$ are the sample mean and standard deviation, respectively, of the non-collapse ln*EDP* results, $\Phi(\cdot)$ denotes the standard normal cumulative distribution function, and $\overline{C}$ denotes 'no collapse.' Combining (2.1) and (2.2) using the total probability theorem, the probability of *EDP* exceeding *z* given $Sa(T_1) = x$ is

$$P\left(EDP > z \mid Sa(T_1) = x\right) = P\left(C \mid Sa(T_1) = x\right) + P\left(\overline{C} \mid Sa(T_1) = x\right)\left(1 - \Phi\left(\frac{\ln z - \hat{\mu}_{\ln EDP|Sa(T_1)=x}}{\hat{\beta}_{\ln EDP|Sa(T_1)=x}}\right)\right) \quad (2.3)$$

Where $P\left(\overline{C} \mid Sa(T_1) = x\right) = 1 - P\left(C \mid Sa(T_1) = x\right)$. This result is used in (1.1), and will be generalized for vector *IM*s in the next section.

3. Prediction of Structural Response Using a Vector IM

A result similar to Eq. (2.3) can be developed for use with a two-element vector *IM*. A vector consisting of $Sa(T_1)$ and $R_{T1,T2}$ is used here to estimate $P(EDP > z \mid Sa(T_1) = x_1, R_{T1,T2} = x_2)$, but the approach can be used with any *IM* parameters of interest. A direct generalization of the above procedure would be to scale the suite of records such that $Sa(T_1) = x_1$ and $R_{T1,T2} = x_2$. Simple amplitude scaling, however, affects all response spectral values equally and leaves spectral shape unmodified; therefore, $R_{T1,T2}$ is unchanged by scaling. It is in general not possible to match two *IM* parameters simultaneously by scaling the amplitude of a ground motion, because only a single scale factor can be specified. Modification of the frequency content of the ground motions could allow for the matching of spectral shape, but it would need to be verified that the resulting response estimates realistically represent the responses of unmodified records with the same spectral shape. The approach used here, instead, is to scale to $Sa(T_1)$ as before and then apply regression analysis to estimate *EDP* as a function of $R_{T1,T2}$ at each $Sa(T_1)$ level. As with the scalar *IM* case, the records causing collapse are dealt with separately, and a probability distribution is fit to the remaining non-collapse responses.

As with the scalar *IM*, some records may cause collapse of the structure. Instead of merely counting the fraction of records that collapse, however, it is now possible to predict the probability of collapse at a given $Sa(T_1)$ level by making the prediction a function of $R_{T1,T2}$ using logistic regression, which is a commonly used tool for predicting binary outcomes [Neter et al. 1996]. If the occurrence of collapse, *C*, is treated as a binary variable equal to 1 if the ground motion causes collapse and 0 otherwise, then the probability of collapse can be predicted as

$$P\left(C \mid Sa(T_1) = x_1, R_{T1,T2} = x_2\right) = \frac{\exp(\hat{\beta}_0 + \hat{\beta}_1 \ln x_2)}{1 + \exp(\hat{\beta}_0 + \hat{\beta}_1 \ln x_2)} \quad (3.1)$$

where the coefficients $\hat{\beta}_0$ and $\hat{\beta}_1$ are estimated using logistic regression on a dataset with records scaled to $Sa(T_1) = x_1$. Example data and the resulting fitted prediction are shown in Figure 2.

The distribution of non-collapse responses is also modeled using regression analysis. It has been observed that the expected value of *EDP* tends to be well-predicted by the function

$$E\left[\ln EDP \mid Sa(T_1)=x_1, R_{T1,T2}=x_2, \overline{C}\right]=\hat{\beta}_2+\hat{\beta}_3 \ln x_2 \tag{3.2}$$

where linear regression is used to obtain estimates of the coefficients, $\hat{\beta}_2$ and $\hat{\beta}_3$ at the given $Sa(T_1)$ level. Graphical examples of this data and regression fits are shown in Figure 3. Using this mean prediction, regression residuals are defined as

$$e_i=\ln EDP_i-\ln \hat{EDP}_i \tag{3.3}$$

where $\ln EDP_i$ is the natural logarithm of the *EDP* associated with record *i*, and $\ln \hat{EDP}_i$ is the prediction from (3.2), based on the record's $R_{T1,T2}$ value. These residuals are assumed to be mutually independent when tests of statistical significance are performed later. In addition, the residuals will be assumed to be normally distributed with constant variance (a condition termed homoscedasticity). These assumptions have been examined for the data in this study, and found to be reasonable. The linear regression prediction of (3.2) is unbiased, so the mean value of the residuals is zero [Neter et al. 1996]. The estimated variance of the residuals, denoted $\hat{Var}[e]\equiv\hat{\sigma}_e^2$, is available from the regression software and is represented graphically in Figure 3 by superimposing the estimated normal distributions of the residuals over the data.

Given the predictive model of (3.2), and given the assumed statistical properties of the residuals, the probability that ln*EDP* is greater than *z*, given $Sa(T_1) = x_1$, $R_{T1,T2} = x_2$, and no collapse can be expressed as

$$P\left(EDP>z \mid Sa(T_1)=x_1, R_{T1,T2}=x_2, \overline{C}\right)=1-\Phi\left(\frac{\ln z-\left(\hat{\beta}_2+\hat{\beta}_3 \ln x_2\right)}{\hat{\sigma}_e}\right) \tag{3.4}$$

This equation is similar to (2.2) used in the scalar case, except that the mean of the normal distribution now comes from the regression prediction based on $R_{T1,T2}$ rather than the average response of all records. The standard deviation of the records has also been replaced by the standard deviation of the regression residuals.

The collapse and non-collapse response predictions from (3.1) and (3.4) can then be combined to compute the probability that *EDP* exceeds *z*

$$P\left(EDP>z \mid Sa(T_1)=x_1, R_{T1,T2}=x_2\right)=P(C)+P\left(\overline{C}\right)\left(1-\Phi\left(\frac{\ln z-\left(\hat{\beta}_2+\hat{\beta}_3 \ln x_2\right)}{\hat{\sigma}_e}\right)\right) \tag{3.5}$$

$$\text{where } P(C)=\frac{\exp(\hat{\beta}_0+\hat{\beta}_1 x_2)}{1+\exp(\hat{\beta}_0+\hat{\beta}_1 x_2)} \text{ and } P\left(\overline{C}\right)=1-P(C)$$

Although x_1 does not appear in (3.5), the equation is implicitly a function of x_1 because the data used to estimate $\hat{\beta}_0$, $\hat{\beta}_1$, $\hat{\beta}_2$, $\hat{\beta}_3$ and $\hat{\sigma}_e$ comes from records scaled to $Sa(T_1)=x_1$. This response prediction is similar to the original prediction of (2.3), but now incorporates a two-element vector. The approach is easily generalized to vectors with more parameters by using regression with multiple predictor variables in (3.1) and (3.2), as will be done in Section 8.

4. Building Models and Ground Motions

Several structural models are used to investigate the effectiveness of vector *IM*s. The primary structure is a 1960's era reinforced concrete moment frame building that is serving as a test-bed for PEER Center research activities [PEER 2004]. A 2D model of the transverse frame is used, which was created by Jalayer [2003] and contains nonlinear elements that degrade in strength and stiffness, in both shear and bending [Pincheira et al. 1999]. The frame has seven stories and three bays. The first mode of the model has a period of 0.8 seconds, and the second mode has a period of 0.28 seconds. The response parameter studied here, maximum interstory drift ratio, is primarily controlled by first-mode response in this structure. Forty historical earthquake ground motions are used for the analysis of the structure [Baker and Cornell 2005b, Table A.1]. The records come from California earthquakes ranging in Magnitude from 5.7 to 7.3, and ranging in distance from 6.5 to 56 km. Attempts were made to avoid directivity effects by choosing records with small distances only when the rupture and site geometry suggested that near-fault effects would be unlikely, and when velocity time histories were not observed to contain pulse-like intervals.

To supplement the results from the primary structure, twenty generic frame models were also analyzed, with a variety of configurations, periods, and degradation properties. The specific model parameters are summarized in Table 1. The structures are single-bay frames, with stiffnesses and strengths chosen to be representative of typical structures. A set of non-degrading models designed and analyzed by Medina and Krawinkler [2005] was considered. These models do not have degrading elements, but can still collapse due to P-Δ effects. Another set of structures were considered that are identical to the models of Medina and Krawinkler except that they incorporate elements that degrade in stiffness and strength [Ibarra 2003, Ibarra *et al.* 2005]. For each of six building configurations, a non-degrading model and two degrading models were considered. For the supplemental generic structures, a different set of 40 records was used for analysis, ranging in magnitude from 6.5 to 6.9 and in distance from 13 to 40 km [Medina and Krawinkler 2003]. The cited authors refer to these records as the LMSR-N set.

5. Choice of T_2 Based on Regression Residuals

With a method to predict structural response and example structures for testing, it is now possible to consider the selection of an effective vector of ground motion parameters for use in prediction. The general goals to be considered when choosing an *IM* are efficiency (minimum variance in *EDP* for records with the same *IM* value), sufficiency [Luco and Cornell 2005], and ease of calculation (e.g., it should be possible to obtain the ground motion hazard for the *IM*, or to determine the *IM* value of a given record).

Sufficiency of an *IM* parameter implies that given knowledge of the *IM* value of a ground motion, structural response is not sensitive to other ground motion parameters of interest. The scalar intensity measure $Sa(T_1)$ has been found to be a sufficient predictor with respect to magnitude and distance [Shome et al. 1998]. This implies that among

ground motions with the same $Sa(T_1)$ value, the magnitude and distance values of the ground motions will not affect the estimated structural response. Sufficiency is a desirable property of an *IM*, because the estimated structural response will not be affected by the specific ground motions used for analysis. Although $Sa(T_1)$ is sufficient with respect to magnitude and distance, Baker and Cornell [2005a] found it to be insufficient with respect to ε (a ground motion parameter that will be discussed later). The vector of $Sa(T_1)$ plus the added parameter $R_{T1,T2}$ retains sufficiency with respect to magnitude and distance, and its sufficiency with respect to ε will be considered in Section 8. Regarding the ease of calculation, the ground motion hazard for this *IM* can be computed [Bazzurro and Cornell 2002], and spectral acceleration values are easy to calculate and familiar to many engineers. With the sufficiency and ease of calculation criteria addressed, T_2 will thus be selected based on efficiency.

The question of efficiency arises when, for example, the mean value of ln*EDP* is considered. A basic result in statistics states that if one has *n* samples from a distribution with standard deviation σ, the standard deviation of the sample mean is proportional to $\sigma/\sqrt{n}$ [Benjamin and Cornell 1970]. Thus, if $\beta_{\ln EDP|IM=x}$ can be decreased by using a more efficient *IM*, then *n* (the number of dynamic analyses performed to obtain response results) can be decreased while estimating the mean ln*EDP* with the same confidence. This will reduce the effort and computational expense associated with the assessment procedure. In Figure 3a and b, $R_{T1,T2}$ parameters producing small and large residual dispersions, respectively, are shown. Clearly fewer data points will be needed to obtain an estimate of ln*EDP* as a function of *IM* when using the efficient $R_{T1,T2}$ from Figure 3a.

This is the motivation for the first method of identifying the optimal T_2 value at a given $Sa(T_1)$ level. Once dynamic analyses have been performed using records scaled to a target $Sa(T_1)$, it is a simple matter to perform regression analysis using $R_{T1,T2}$ for a range of T_2 values and compute the standard deviations of the resulting residuals. To measure the benefit of the vector *IM* relative to $Sa(T_1)$, the fractional reduction in the standard deviation of the prediction errors relative to the standard deviation from the case with $Sa(T_1)$ alone can be computed. The T_2 causing the largest fractional reduction will be identified as optimal under this criterion.

6. Optimal T_2 Results Based on Regression Residuals

Using the primary test structure and associated ground motions, candidate T_2 values for $R_{T1,T2}$ can be evaluated. A plot of the fractional reduction in residual standard deviation is shown in Figure 4, where all records have been scaled to $Sa(T_1) = 0.3g$. The optimal T_2 is one second (i.e., $T_2/T_1 = 1.25$), and the reduction in dispersion is approximately 60%. Note that this optimal T_2 at this spectral acceleration level was used to create Figure 3a, and a less effective T_2 was used for Figure 3b. Using the rule that the standard deviation of the sample mean is $\sigma/\sqrt{n}$, a 60% reduction in standard deviation indicates that the number of records analyzed could be potentially reduced by a factor of six while maintaining the same confidence in the mean estimate, leading to a great reduction in

computational expense. This T_2 value is associated with a single level of $Sa(T_1)$. The same calculation can be repeated at other levels, and results for two additional levels of $Sa(T_1)$ are shown in Figure 5, where it is apparent that the optimal T_2 value varies depending on the level of $Sa(T_1)$. An additional value, $\tilde{\mu}$, is given in the legend. This is the ratio of the geometric mean maximum interstory drift ratio among the 40 responses to the maximum interstory drift ratio at yielding (as determined from a pushover analysis of the structure), and is analogous to a ductility level for the structure.

At $Sa(T_1) = 0.1g$ the optimal T_2 is 0.36 seconds, and at 0.28 seconds—the second-mode period of the structure—the reduction in dispersion is nearly as large. A vector *IM* with T_2 equal to the structure's second-mode period is related to the modal analysis method of estimating linear response, which uses spectral acceleration at elastic modal periods to estimate structural response. At this level of spectral acceleration, $\tilde{\mu}$ is 0.533, implying that the structure stays linear for most of the records. For $Sa(T_1) = 0.3g$, the optimal T_2 is 1.0 seconds as discussed above. It is noted now that $\tilde{\mu} = 1.56$, suggesting that most of the records cause some level of nonlinear behavior in the structure. For $Sa(T_1) = 0.7g$, the optimal T_2 is 1.5 seconds. At this level of spectral acceleration, $\tilde{\mu} = 4.66$. This indicates that most of the records experience large levels of nonlinearity. Other authors have examined the choice of T_2 for similar applications, and have also recognized the dependence on the level of nonlinearity [Cordova *et al.* 2001, Vamvatsikos and Cornell 2005].

In Figure 6, the level of $Sa(T_1)$ is plotted versus the ratio of T_2 to T_1. Circles indicate the optimal T_2 for a given $Sa(T_1)$ and vertical lines indicate the range of T_2/T_1 where the reduction in dispersion is at least 75% of the reduction seen at the optimal T_2. These lines are shown to indicate whether there are only a few effective T_2 values or whether there is a large range of T_2 values that reduce dispersion comparably.

The structure's $\tilde{\mu}$ is less than one for $Sa(T_1)$ between 0 and $0.1g$, and there the optimal T_2 is near the second-mode period of the building. For $Sa(T_1) \geq 0.2g$, where $\tilde{\mu} > 1$, the optimal T_2 is larger than T_1 and shows an increasing trend as $Sa(T_1)$ increases (and levels of nonlinearity increase). The dependence of T_2 on the level of nonlinearity is similar to the concepts from equivalent linear systems, where a nonlinear single-degree-of-freedom system is represented by an 'equivalent' linear system with a lengthened period. As the level of nonlinearity increases, the period of the equivalent linear system increases. Predictions of equivalent periods for nonlinear systems based on level of nonlinearity have been proposed by, for example, Iwan [1980] and Kennedy [1985]. These predictions show trends similar to the effective T_2's seen in this study, as illustrated in Figure 6. There is one difference, however, between the period of an equivalent linear system and the T_2 being selected for use in a vector *IM*. An equivalent linear system is used to *replace* $Sa(T_1)$, while here the IM_2 is used to *supplement* $Sa(T_1)$. This discrepancy is seen in Figure 6 when $Sa(T_1)$ is 0.3 or $0.4g$. Here the equivalent nonlinear system has a period almost identical to the elastic period of structure, while the optimal T_2 from this study is at a longer period. This is because if T_2 is near to T_1, then $Sa(T_1)$ is highly correlated with $Sa(T_2)$ [Baker and Cornell 2006b]; $R_{T1,T2} = Sa(T_2) / Sa(T_1)$

is thus essentially constant for all records and so provides little useful information. The optimal T_2 must differ significantly from T_1 in order to decrease the correlation between $Sa(T_1)$ and $Sa(T_2)$. This is apparent in Figure 5, where the fractional reduction in dispersion is always very low for T_2 values close to T_1. So although there is some similarity between optimal T_2 values for this vector *IM* and periods of equivalent linear systems, the two concepts differ, especially at low levels of nonlinearity.

The same search for optimal periods was performed with the generic frame structures. Because these structures have differing first-mode periods and yield *Sa* levels, $Sa(T_1)$ is normalized to allow uniform display of the results. Here the $Sa(T_1)$ level is chosen so that the records' $Sa(T_1)$ level in units of *g* is a specified multiple of the structure's base shear coefficient γ (where γ=yield base shear/weight). The ratio $Sa(T_1) / \gamma$ is analogous to an R-factor in present building codes, if there were no overstrength in the structure; here it will be referred to as R_μ. With this measure, nonlinear behavior starts occurring at an R_μ value of approximately one for all structures, although higher-mode response will alter the exact point of yielding somewhat [Medina and Krawinkler 2003]. Further, the optimal T_2 is normalized by the first-mode period of the structure as was done in Figure 6. These normalizations allow multiple structures to be plotted on the same figure for comparison, independent of their first-mode period or yield strength. The structures are separated into four groups for consideration.

The first group, shown in Figure 7a, consists of three-story structures with peak interstory drift ratios controlled primarily by first-mode response. Here the optimal T_2 is in many cases near to the second-mode period of the structure when the structure is linear (R_μ <1) or slightly nonlinear. In the moderately nonlinear range, however, the optimal period is typically larger than the first-mode period and increases as the ground motion intensity increases. The general trends in Figure 7a are similar to the trend in Figure 6. The second group of structures, shown in Figure 7b, have peak interstory drift ratios that are moderately sensitive to second-mode response. In the linear range, the optimal T_2 is again near the second-mode period. Here, however, the optimal T_2 is near the second-mode period for normalized *Sa* values up to four in several cases. The third group of structures, shown in Figure 7c, have peak interstory drift ratios that are significantly affected by second-mode response—more-so than most typical buildings [Helmut Krawinkler, personal communication 2005]. Here the optimal T_2 is almost always near the second-mode period. The final group of structures, shown in Figure 7d, all have nine stories and a first-mode period of 0.9 seconds, but have varying ductility capacities (δ_c/δ_y). Each of these structures undergoes a transition from having an optimal T_2 less than T_1 to having an optimal T_2 greater than T_2 at an R_μ factor between 3.5 and 6.5. The structures with lower ductility capacity undergo this transition at a lower R_μ level; this is likely because structures with low ductility are more sensitive to long-period excitations that may drive them to extreme responses. Ductile structures may be more able to withstand these long-period excitations, and thus information about higher mode response may be more important in this transition region. At large enough *Sa* levels, all four of these structures are sensitive to long-period T_2's; the low-ductility structures

merely make the transition sooner. It is interesting to note that for several of the structures in Figure 7b-d, the optimal T_2 in the nonlinear response range is less than T_1 but larger than the elastic second-mode period. This suggests that the effective second-mode period may be lengthening due to nonlinearity [Fu 2005], although no further analysis was performed to confirm this.

Some general conclusions might be inferred from these empirical results. When the structure is significantly affected by second-mode response (i.e., either the structure is behaving linearly or second-mode response is a strong contributor to response even in the nonlinear range), then the optimal T_2 is typically near the elastic second-mode period. When the structure is behaving nonlinearly and second-mode response is not critical, the optimal T_2 is typically larger than the elastic first-mode period. In addition, low-ductility structures may have optimal T_2 values longer than the first-mode period at lower *Sa* levels than high ductility structures. These trends are all consistent with engineering intuition about dynamic structural response, but the observed results are not yet general enough to develop concrete rules for optimal T_2 values. A rule-of-thumb approach based on the results here might be to use a T_2 equal to the second-mode period when second mode response is most important, and to use a T_2 equal to twice the first-mode period when nonlinear response is expected to be important.

It is helpful to reconsider the initial scheme for predicting *EDP* as a function of two *IM* parameters, in light of the previous results. There are a variety of methods for making this prediction [Baker 2007], but here the choice was made to first scale records to $Sa(T_1)$ and then regress on $R_{T1,T2}$. The regression coefficients vary at each $Sa(T_1)$ level, allowing for full interaction between $Sa(T_1)$ and $R_{T1,T2}$. If regression predictions had been made using un-scaled records with both $Sa(T_1)$ and $R_{T1,T2}$ as predictors, it would have been more difficult to identify the interaction between the two parameters. In addition, simultaneous regression on both $Sa(T_1)$ and $R_{T1,T2}$ eliminates the possibility of studying how the optimal T_2 varies as a function of $Sa(T_1)$. For these two reasons, scaling to $Sa(T_1)$ and then regressing on $R_{T1,T2}$ was chosen as the preferred approach here. The advantage of regressing on two *IM* parameters simultaneously, as was done by Shome [1999], is that there are fewer parameters to estimate. Only one set of coefficients is needed for the entire range of $Sa(T_1)$ and $R_{T1,T2}$, rather than a new set of coefficients for $R_{T1,T2}$ at each $Sa(T_1)$ stripe, potentially reducing the number of analyses needed for parameter estimation. Thus, the simultaneous regression approach may be appealing for practical applications, but the approach used here was deemed more useful for exploratory research.

7. Choice of T_2 Using the Bootstrap and the Drift Hazard Curve

The methodology used thus far for choosing an optimal $R_{T1,T2}$ has one weakness. Recall that the quantity being optimized in Figure 4 is the reduction in residual dispersion from regression on the *non-collapse* responses. The ability of $R_{T1,T2}$ to predict the probability of collapse is not measured. Because of this, the plot of Figure 6 was limited to $Sa(T_1) \leq 1g$.

When $Sa(T_1) > 1g$, more than one-quarter of the ground motions cause this structure to collapse, so a criterion based solely on non-collapse responses is not appropriate. Ideally, the quantity to optimize should account for improvements made in prediction of both collapse *and* non-collapse responses.

A natural way to resolve this issue is to carry the prediction of *EDP* through to the computation of the rate of exceeding an *EDP* value *z*, as discussed in the introduction. This result is sometimes referred to as a drift hazard curve. The vector version of (1.1) is given by

$$\lambda_{EDP}(z) = \sum_{\text{all } x_{1,i}} \sum_{\text{all } x_{2,i}} P\left(EDP > z \mid Sa(T_1) = x_{1,i}, R_{T1,T2} = x_{2,i}\right) \cdot \Delta\lambda_{IM}\left(x_{1,i}, x_{2,i}\right) \quad (7.1)$$

The estimate will vary depending upon the records chosen for analysis, although with an efficient *IM* the estimate will not vary by much. Thus, a reduction in sensitivity to the records chosen here would be a good criterion to use in selecting $R_{T1,T2}$. This criterion addresses both the efficiency and sufficiency issues described earlier, as well as accounting for collapse and non-collapse responses. To measure the statistical variability of the estimate of $\lambda_{EDP}(z)$, one can employ the bootstrap [Efron and Tibshirani 1993]. This procedure is performed as follows: select *n* records *with replacement* from the original set of *n* records (some records will be duplicated and others not present at all). With the new set of records and their previously calculated associated responses, use a vector *IM* with the candidate $R_{T1,T2}$ to predict the building response as before. Using the new estimate, re-compute $\lambda_{EDP}(z)$ using (7.1). Repeat this process *B* times (typically 25 to 200). The standard deviation of these *B* values is an estimate of the standard error of estimation of $\lambda_{EDP}(z)$. No new structural analyses are needed for this process, so the computational expense is not large. A good T_2 value for $R_{T1,T2}$ will result in a $\lambda_{EDP}(z)$ with significantly reduced variability relative to the $\lambda_{EDP}(z)$ calculated with Eq. (1.1) using a scalar *IM*. There are two advantages introduced by this method. First, it incorporates both the collapse and non-collapse predictions naturally into the final computation where the results will be used. Second, this criterion measures efficiency gains over the entire range of $Sa(T_1)$ values that are related to the given *EDP* level, rather than at just a single $Sa(T_1)$ value. Note that this calculation requires the ability to perform a vector-valued ground motion hazard analysis to determine $\Delta\lambda_{IM}(x_{1,i}, x_{2,i}) = \lambda_{Sa(T_1)\in[x_{1,i}, x_{1,i+1}], R_{T1,T2}\in[x_{2,i}, x_{2,i+1}]}$. This result can be approximately thought of as the annual rate of $Sa(T_1) = x_{1,i}$ and $R_{T1,T2} = x_{2,i}$. This type of hazard analysis can be computed [Bazzurro and Cornell 2002, Somerville and Thio 2003], but is not yet widely used in engineering practice.

To illustrate this concept, the complete drift hazard curve $\lambda_{EDP}(z)$ is computed using the scalar and vector procedures (Eq. (1.1) and (7.1) respectively). The ground motion hazard is calculated for the actual location of the structure being studied (a stiff-soil site near Los Angeles, California). The scalar and vector-based results are shown in Figure 8. Note that the flattening of the curve towards the right occurs because the exceedance of these *EDP* values is dominated by collapses ($P(C) \cong 0.003$). There is not a large difference between the two curves, but what cannot be seen in this figure is that there is much less uncertainty in the curve estimated using the vector *IM*. This uncertainty can be

measured using the bootstrap. The vector-*IM*-based drift hazard curves computed from four example bootstrap replicates are shown in Figure 9. The variability among the bootstrapped drift hazard estimates indicates the degree to which the result is sensitive to the records selected, due to a lack of efficiency or sufficiency in the *IM*. The coefficient of variation of 200 bootstrapped curves is computed for a range of *EDP* levels using several *IM*s, and shown in Figure 10. The vector consisting of $Sa(T_1)$ and $R_{T1,T2}$, with T_2 = 1.0s, produces a significant reduction in coefficient of variation for nearly all levels of *IM*, with a 50% reduction in the range $0.003 < EDP < 0.01$. The other two vectors do not show a significant improvement. This result fits with results seen earlier. The vector with T_2 = 0.28s was only helpful for very small levels of $Sa(T_1)$, as seen in Figure 6. The vector with T_2 = 2.0s was helpful as $Sa(T_1)$ levels got very large, but these large-intensity events are rare enough that they do not significantly affect the *EDP* hazard curve except at large levels of *EDP*. The vector with T_2 = 1.0s showed an improvement over a large range of important $Sa(T_1)$ levels, and thus appears to be the most useful here. These bootstrap-based results are consistent with the earlier results, but perhaps this method reveals more information about the overall usefulness of a candidate vector than the previous method. Note that the best vector may depend upon the *EDP* level of interest, whereas previously the best vector was conditional upon the $Sa(T_1)$ level.

This bootstrap procedure requires more computational effort than the regression procedure, but it has the advantage of directly measuring uncertainty in the parameter of great interest, $\lambda_{EDP}(z)$, and incorporating estimates from both collapse and non-collapse prediction at multiple *IM* levels simultaneously. Research to date seems to indicate that the two alternative procedures identify similar T_2 values at levels of *EDP* where collapses are not frequent.

8. A Three-Parameter Vector Consisting of $Sa(T_1)$, $R_{T1,T2}$ and ε

The ground motion parameter ε has been a subject of recent investigations [Baker and Cornell 2005a, 2006a], and has been found to predict structural response given knowledge of $Sa(T_1)$. This parameter is a measure of the difference between a ground motion's $Sa(T_1)$ value and the mean $Sa(T_1)$ from a ground motion prediction equation. Records with positive ε values tend to have 'peaks' in their spectra at the specified period, and negative ε values are associated with 'valleys.' This means that ε is an indicator of spectral shape, and explains why it predicts structural response. Because ε and $R_{T1,T2}$ both relate to spectral shape, the possibility exists that they are accounting for the same effect. If they do account for the same effect, then use of a vector with $R_{T1,T2}$ would eliminate the need to carefully account for the effect of ε. A vector consisting of three parameters—$Sa(T_1)$, $R_{T1,T2}$ and ε—is used to investigate this possibility. The question to be answered is whether this three-parameter *IM* is better than the two-parameter *IM* consisting of $Sa(T_1)$ and $R_{T1,T2}$. To test this, we first perform scaling on $Sa(T_1)$ stripes, as in Section 3. The only modification needed is that the regressions now

use two predictor variables. The prediction of collapse is analogous to (3.1), but now with an added term for ε

$$P\left(C \mid Sa(T_1) = x_1, R_{T1,T2} = x_2, \varepsilon = x_3\right) = \frac{\exp(\hat{\beta}_0 + \hat{\beta}_1 \ln x_2 + \hat{\beta}_2 x_3)}{1 + \exp(\hat{\beta}_0 + \hat{\beta}_1 \ln x_2 + \hat{\beta}_2 x_3)} \tag{8.1}$$

The prediction of mean response of non-collapse records is performed using the function

$$E\left[\ln EDP \mid Sa(T_1) = x_1, R_{T1,T2} = x_2, \varepsilon = x_3, \bar{C}\right] = \hat{\beta}_3 + \hat{\beta}_4 \ln x_2 + \hat{\beta}_5 x_3 \tag{8.2}$$

where the coefficients $\hat{\beta}_0$ through $\hat{\beta}_5$ are again estimated using a dataset with records that have been scaled to $Sa(T_1) = x_1$. These results are then combined in a manner similar to that of (3.5), and the drift hazard is computed using

$$\lambda_{EDP}(z) = \sum_{\text{all } x_{1,i}} \sum_{\text{all } x_{2,i}} \sum_{\text{all } x_{3,i}} \left[\begin{array}{l} P(EDP > z \mid Sa(T_1) = x_{1,i}, R_{T1,T2} = x_{2,i}, \varepsilon = x_{3,i}) \\ \cdot \Delta\lambda_{IM}(x_{1,i}, x_{2,i}, x_{3,i}) \end{array} \right] \tag{8.3}$$

The three-parameter ground motion hazard and the three-parameter *IM* response prediction have both been computed for the first time as part of this study.

To determine whether the predictions incorporating ε are significantly superior to predictions that do not include ε, a statistical test known as the F-test is used [Neter et al. 1996]. For a given structure and $Sa(T_1)$ level, both the full model incorporating $R_{T1,T2}$ and ε (Eq. (8.1) and (8.2)) and the reduced model without ε (Eq. (3.1) and (3.2)) are fitted. A measure of the improvement in fit from the reduced model to the full model, called an F statistic, is computed. The probability of exceeding that F statistic under the assumption that ε is not significant is called a p-value. Low p-values suggest that the effect of ε is significant, because they indicate that the observed level of improvement in fit is unlikely to occur under the assumption that ε is not significant. A p-value of less than 0.05 is typically interpreted as indicating that ε has a statistically significant effect. P-values from a subset of the test results are displayed in Table 2. In all, approximately 25% of the tests show p-values below 0.05, versus the expected 5% under the assumption that ε is not significant. This suggests that ε is still a mildly significant predictor of structural response as a third parameter in addition to $Sa(T_1)$ and $R_{T1,T2}$. Note that among the results with approximately linear ($R_\mu \leq 1$) response, ε is very significant for the 0.6s and 0.9s structures when T_2 is chosen to be longer than the first-mode period of the building. When T_2 is chosen at the second-mode period of the building, ε is no longer significant for these same structures. This suggests that ε is predicting response of the second mode: ε is only significant if the $R_{T1,T2}$ is not chosen to account for the second-mode response. The same effect is not present with the 0.3 second structure, perhaps because the second mode of this structure does not contribute significantly to response.

Drift hazard curves computed using several candidate *IM*s are shown in Figure 11. The *IMs* including ε as a parameter produce lower estimates of the mean annual rate of exceedance at large maximum interstory drift ratios. Because the addition of ε to the *IM* affects the drift hazard results, it can be inferred that $R_{T1,T2}$ is not fully accounting for the effect of ε.

The ability of $R_{T1,T2}$ and ε to predict spectral shape at a range of periods is shown in Figure 12. The procedure used to create this plot is as follows. Forty ground motions were scaled so that they all had the same Sa(0.8s) value. The parameters ε and $R_{T1,T2}$ were then used to predict spectral acceleration values at a range of periods using linear regression. The standard deviations of the prediction residuals were compared to the standard deviation of the spectral values before prediction to indicate the ability of the *IM* parameters to explain variations in the response spectrum. $R_{T1,T2}$ by definition explains 100% of the variation at the period T_2 (1 sec. in this figure), and at other periods it has a lesser predictive ability. In particular, $R_{T1,T2}$ with this $T_2 > T_1$ has almost no predictive power at periods less than T_1, as might be expected. On the other hand, ε has at least some predictive power over almost the entire range of periods considered. Judging from this figure, it appears that ε and $R_{T1,T2}$ are not explaining the same features of spectral shape. In particular, ε predicts spectral values on either side of T_1, while $R_{T1,T2}$ predicts only on one side. This may explain why the predictions based on the three-parameter vector of $Sa(T_1)$, $R_{T1,T2}$ and ε are different than the predictions based on $Sa(T_1)$ and $R_{T1,T2}$. Additionally, unpublished research by the authors indicates that when the median spectral shape of the records used for structural analysis is inconsistent with the spectral shape predicted by the ground motion prediction (attenuation) model used for hazard analysis, an inconsistency in the resulting drift hazard is introduced. This may explain the discrepancy between the two-parameter and three-parameter drift hazard curves in Figure 11. Further investigation is needed into this phenomenon, however, before firm conclusions can be drawn.

Using the bootstrap procedure, the coefficients of variation were computed for each drift hazard curve in Figure 11; the results are shown in Figure 13. Interestingly, the coefficients of variation of $\lambda_{EDP}(z)$ increase somewhat when ε is included as an *IM* parameter. The ε-based predictions normally require some extrapolation, because mean ε values for randomly selected ground motions are near zero while ground motion intensities of interest for safety assessment are often caused by ground motions with ε values of one to two, at least in seismically active regions such as the California site considered here [Baker and Cornell 2005a]. This extrapolation, as well as the need to estimate additional regression coefficients, introduces additional model uncertainty into the predictions; it appears that the reduction in standard deviation of response residuals achieved by ε (a lesser reduction than is achieved by $R_{T1,T2}$) is not large enough to offset this increase in model uncertainty.

Although ε slightly increases the coefficient of variation of estimation for of the drift hazard curve when used in an *IM*, it has also been seen to eliminate a source of bias associated with use of $Sa(T_1)$ alone [Baker and Cornell 2005a]. This is the reason why the drift hazard curves in Figure 11 that incorporate ε are lower. The parameter $R_{T1,T2}$ by itself is not able to eliminate this bias, so it still suggested that ε be included in probabilistic performance assessments. The increased coefficient of variation of $\lambda_{EDP}(z)$ could be avoided, however, by using ε-based record selection rather than random selection and an *IM* that includes ε [Baker and Cornell 2006a].

The results from this section suggest that use of a vector-valued *IM* consisting of $Sa(T_1)$ and $R_{T1,T2}$ does not desensitize the analysis to the effects of ε. Although ε and $R_{T1,T2}$ are both effective *IM* parameters because they are related to spectral shape, they describe somewhat different properties of the shape of the spectrum. Further, these two parameters have different effects on estimated drift hazard curves: a vector *IM* with $R_{T1,T2}$ tends to reduce the uncertainty in the curve relative to results obtained with a scalar *IM*, while a vector *IM* with ε tends to eliminate a bias in the drift hazard. The parameter ε should thus still be accounted for, as its effect is significant, especially at large levels of response.

9. Conclusions

Methods for selecting and using efficient vector-valued ground motion intensity measures have been presented. Two *IM* parameters were given primary consideration: elastic spectral acceleration, $Sa(T_1)$, and a measure of spectral shape, $R_{T1,T2} = Sa(T_2) / Sa(T_1)$. The period T_1 was fixed as the first-mode period of the structure considered, and methods for identifying a useful T_2 were considered here. The first method was based on scaling ground motions to the target level of $Sa(T_1)$ and using regression on $R_{T1,T2}$ to predict the response of the structure. The optimal T_2 for use in the vector was then chosen by minimizing the standard deviation of the prediction errors. It was shown that when chosen effectively, $R_{T1,T2}$ can reduce the standard deviation of the prediction errors by up to 60% when compared to prediction using $Sa(T_1)$ alone. A variety of nonlinear MDOF structures were tested to find the optimal second period for use in this *IM*. When the building response was linear or when nonlinear building response has a significant contribution from the second mode of vibration, the optimal second period for use in $R_{T1,T2}$ is often approximately equal to the second-mode period of the building. When $Sa(T_1)$ was large enough to cause nonlinear behavior and second-mode response was not critical, the optimal second period was larger than the first-mode period of the building. As a rule of thumb, a T_2 equal to twice the level of the elastic first mode period agrees reasonably with the results seen here, and is consistent with similar conclusions by other researchers [Cordova *et al.* 2001].

A second method for evaluating vector *IMs,* which utilizes bootstrap replications of the drift hazard curve, was also presented. This method has the advantage of directly computing the statistical variability in estimates of the drift hazard curve, and it accounts for the increased prediction efficiency of both collapse and non-collapse responses at many *IM* levels simultaneously. A disadvantage of this approach is that it requires a vector-valued ground motion hazard calculation for each candidate *IM*, and it also requires slightly increased computational time. Because of this, it is suggested that the regression analysis method be used to narrow down a broad range of potential vector *IMs* to a few promising candidates. The bootstrap method can then be used to examine these few in detail.

A three-parameter *IM* consisting of $Sa(T_1)$, $R_{T1,T2}$ and ε was considered to determine whether $R_{T1,T2}$ accounted for the effect of ε—a ground motion parameter identified in recent research as being important. It was seen that $R_{T1,T2}$ does not fully account for the effect of ε, and that neglecting ε in analysis results in conservative estimates of the annual rate of exceeding a given maximum interstory drift ratio, especially at large levels of structural response. Although the parameter $R_{T1,T2}$ produces significant increases in estimation efficiency, it apparently is not able to account for the effect of ε.

A vector-valued intensity measure consisting of $Sa(T_1)$ and $R_{T1,T2}$ has the potential to produce a drift hazard curve with significantly narrower confidence bands than the equivalent curve computed using the scalar intensity measure $Sa(T_1)$ and the same number of nonlinear analyses. Analyses performed here indicate the potential for a reduction in the standard deviation of $\lambda_{EDP}(z)$ of as much as a factor of two. This implies that in principle, the required number of analyses could be reduced by a factor of as much as four without increasing the standard deviation of the $\lambda_{EDP}(z)$ result.

The subjects of vector-valued *IMs*, estimates of uncertainty in $\lambda_{EDP}(z)$, and record selection with respect to ε are all relatively new. The joint effects of these topics, such as $\lambda_{EDP}(z)$ estimation uncertainty when ε-based record selection is used, require further study.

Acknowledgements

This work was supported primarily by the Earthquake Engineering Research Centers Program of the National Science Foundation, under Award Number EEC-9701568 through the Pacific Earthquake Engineering Research Center (PEER). We thank our co-researchers Dr. Paul Somerville and Dr. Hong Kie Thio for providing the vector-valued ground motion hazard results.

References

Aslani, H. and Miranda, E., [2003]. "Probabilistic response assessment for building-specific loss estimation", Pacific Earthquake Engineering Research Center, University of California at Berkeley, PEER 2003-03, Berkeley, California.

Baker, J. W. and Cornell, C. A., [2005a]. "A vector-valued ground motion intensity measure consisting of spectral acceleration and epsilon," *Earthquake Engineering & Structural Dynamics* **34** (10), 1193-1217.

Baker, J. W. and Cornell, C. A., [2005b]. "Vector-valued ground motion intensity measures for probabilistic seismic demand analysis", John A. Blume Earthquake Engineering Center, John A. Blume Earthquake Engineering Center Report No. 150, Report #150, Stanford, CA. http://blume.stanford.edu/Blume/Publications.htm

Baker, J. W. and Cornell, C. A., [2006a]. "Spectral shape, epsilon and record selection," *Earthquake Engineering & Structural Dynamics* **35** (9), 1077–1095.

Baker, J. W. and Cornell, C. A., [2006b]. "Correlation of response spectral values for multi-component ground motions," *Bulletin of the Seismological Society of America* **96** (1), 215-227.

Baker, J. W., [2007]. "Probabilistic structural response assessment using vector-valued intensity measures," *Earthquake Engineering & Structural Dynamics* **36** (13), 1861 - 1883.

Bazzurro, P. and Cornell, C. A., [2002]. "Vector-valued probabilistic seismic hazard analysis", *7th U.S. National Conference on Earthquake Engineering*, Boston, MA, 10 pp.

Benjamin, J. R. and Cornell, C. A., [1970]. *Probability, statistics, and decision for civil engineers*, (McGraw-Hill, New York).

Cordova, P. P., Deierlein, G. G., Mehanny, S. S. F., and Cornell, C. A., [2001]. "Development of a two-parameter seismic intensity measure and probabilistic assessment procedure", *The Second U.S.-Japan Workshop on Performance-Based Earthquake Engineering Methodology for Reinforced Concrete Building Structures*, Sapporo, Hokkaido, 187-206 pp.

Cornell, C. A. and Krawinkler, H., [2000]. "Progress and challenges in seismic performance assessment," *PEER Center News* **3** (2).

Efron, B. and Tibshirani, R. J., [1993]. *An introduction to the bootstrap*, (Chapman & Hall, New York).

Fu, Q., [2005]. *Modeling and prediction of fault-normal near-field ground motions and structural response*, (Stanford University, *Ph.D. Thesis*, Stanford, CA).

Ibarra, L. F., [2003]. *Global collapse of frame structures under seismic excitations*, (Stanford University, *Ph.D. Thesis*, Stanford, CA).

Ibarra, L. F., Medina, R. A., and Krawinkler, H., [2005]. "Hysteretic models that incorporate strength and stiffness deterioration," *Earthquake Engineering & Structural Dynamics* **34** (12), 1489-1511.

Iwan, W. D., [1980]. "Estimating inelastic response spectra from elastic response spectra," *Earthquake Engineering & Structural Dynamics* **8**, 375-388.

Jalayer, F., [2003]. *Direct probabilistic seismic analysis: Implementing non-linear dynamic assessments*, (Stanford University, *Ph.D. Thesis*, Stanford, CA). http://www.stanford.edu/group/rms/ (accessed 3/14/05)

Kennedy, R. P., Kincaid, R. H., and Short, S. A., [1985]. "Prediction of inelastic response from elastic response spectra considering localized nonlinearities and soil-structure interaction", *8th SMIRT*, 427-434 pp.

Luco, N. and Cornell, C. A., [2005]. "Structure-specific scalar intensity measures for near-source and ordinary earthquake ground motions," *Earthquake Spectra (Under revision for publication)*.

Medina, R. A. and Krawinkler, H., [2003]. *Seismic demands for nondeteriorating frame structures and their dependence on ground motions*, (Stanford University, *John A. Blume Earthquake Engineering Center Report No. 144*, Stanford, CA).

Medina, R. A. and Krawinkler, H., [2005]. "Evaluation of drift demands for the seismic performance assessment of frames," *Journal of Structural Engineering* **131** (7), 1003-1013.

Neter, J., Kutner, M. H., Nachtsheim, C. J., and Wasserman, W., [1996]. *Applied linear statistical models*, (McGraw-Hill, Boston).

PEER*Testbeds project site, http://www.peertestbeds.net*. 2004.

Pincheira, J. A., Dotiwala, F. S., and D'Souza, J. T., [1999]. "Seismic analysis of older reinforced concrete columns," *Earthquake Spectra* **15** (2), 245-272.

Shome, N., Cornell, C. A., Bazzurro, P., and Carballo, J. E., [1998]. "Earthquakes, records, and nonlinear responses," *Earthquake Spectra* **14** (3), 469-500.

Shome, N., [1999]. *Probabilistic seismic demand analysis of nonlinear structures*, (Stanford University. http://www.stanford.edu/group/rms/

Shome, N. and Cornell, C. A., [2000]. "Structural seismic demand analysis: Consideration of "Collapse"", *8th ASCE Specialty Conference on Probabilistic Mechanics and Structural Reliability*, University of Notre Dame, South Bend, Indiana, 7 pp.

Somerville, P. G. and Thio, H. K., [2003]. "Probabilistic vector-valued ground motion intensity measures and engineering demand measures for the PEER van nuys holiday inn PBEE testbed." SCEC 2003 Project Report.

Vamvatsikos, D. and Cornell, C. A., [2005]. "Developing efficient scalar and vector intensity measures for IDA capacity estimation by incorporating elastic spectral shape information," *Earthquake Engineering & Structural Dynamics* **34** (13), 1573-1600.

Table 1. Element properties used for the 20 generic frame structures considered. The parameters are defined as follows [Ibarra 2003]: T_1 is the period of the first mode of vibration, δ_c/δ_y is ductility capacity (displacement at peak strength divided by yield displacement), α_c is post-capping stiffness, and $\gamma_{s,c,k,a}$ quantifies the rate of (hysteretic-energy-based) deterioration. All structures have a post-yield stiffness of 0.03 times the elastic stiffness and a peak-oriented hysteretic model.

Number of stories	**T_1**	**δ_c/δ_y**	**α_c**	**Cyclic deterioration parameters**
3	0.3	4	-0.1	$\gamma_{s,c,k,a}=\infty$
3	0.3	4	-0.5	$\gamma_{s,c,k,a}=50$
3	0.3	∞	-	$\gamma_{s,c,k,a}=\infty$
3	0.6	4	-0.1	$\gamma_{s,c,k,a}=\infty$
3	0.6	4	-0.5	$\gamma_{s,c,k,a}=50$
3	0.6	∞	-	$\gamma_{s,c,k,a}=\infty$
6	0.6	4	-0.1	$\gamma_{s,c,k,a}=\infty$
6	0.6	4	-0.5	$\gamma_{s,c,k,a}=50$
6	0.6	∞	-	$\gamma_{s,c,k,a}=\infty$
9	0.9	2	-0.1	$\gamma_{s,c,k,a}=\infty$
9	0.9	4	-0.1	$\gamma_{s,c,k,a}=\infty$
9	0.9	6	-0.1	$\gamma_{s,c,k,a}=\infty$
9	0.9	4	-0.5	$\gamma_{s,c,k,a}=50$
9	0.9	∞	-	$\gamma_{s,c,k,a}=\infty$
9	1.8	4	-0.1	$\gamma_{s,c,k,a}=\infty$
9	1.8	4	-0.5	$\gamma_{s,c,k,a}=50$
9	1.8	∞	-	$\gamma_{s,c,k,a}=\infty$
15	3	4	-0.1	$\gamma_{s,c,k,a}=\infty$
15	3	4	-0.5	$\gamma_{s,c,k,a}=50$
15	3	∞	-	$\gamma_{s,c,k,a}=\infty$

Table 2. P-values for tests of significance of ε, given $Sa(T_1)$ and $R_{T1,T2}$. Tests were performed using the generic structures with the following parameter values: δ_c/δ_y=4, α_c=-0.1 and $\gamma_{s,c,k,a}$=∞ (see Table 1). Linear regression tests were only performed when at least 10 records did not cause collapse. Logistic regression tests were only performed when at least 5 records caused collapse *and* at least 5 records did not cause collapse. Tests indicating statistical significance (p<0.05) are marked in bold, and '-' indicates that the test was not performed.

		Linear regression						**Logistic regression**					
Number of stories		3	6	9	3	6	9	3	6	9	3	6	9
T_1		0.3	0.6	0.9	0.3	0.6	0.9	0.3	0.6	0.9	0.3	0.6	0.9
T_2 for $R_{T1,T2}$		T_1/3			T_1*2			T_1/3			T_1*2		
R_μ	0.5	0.61	0.97	0.97	0.87	**0.00**	**0.00**	-	-	-	-	-	-
	1	0.61	0.97	0.97	0.87	**0.00**	**0.00**	-	-	-	-	-	-
	1.5	**0.02**	0.15	0.57	**0.03**	**0.01**	**0.00**	-	-	-	-	-	-
	2	**0.05**	**0.02**	0.93	**0.03**	**0.02**	**0.00**	-	-	-	-	-	-
	2.5	0.41	**0.03**	0.64	0.31	0.11	**0.03**	-	-	-	-	-	-
	3	0.24	0.05	0.88	0.18	0.25	0.06	0.25	-	-	0.52	-	-
	3.5	0.77	0.14	0.13	0.59	0.59	**0.03**	**0.05**	-	-	0.06	-	-
	4	0.62	0.19	**0.04**	0.45	0.07	0.08	0.09	-	-	0.12	-	-
	4.5	-	0.07	**0.04**	-	**0.01**	0.15	**0.03**	-	-	**0.03**	-	-
	5	-	0.74	0.12	-	0.27	0.46	**0.01**	0.07	0.11	**0.02**	**0.04**	0.67
	5.5	-	0.91	0.16	-	0.67	0.32	**0.04**	**0.04**	0.07	**0.03**	**0.02**	0.61
	6	-	0.45	0.06	-	0.41	0.16	0.07	0.14	0.16	0.07	0.08	0.97
	7	-	-	0.60	-	-	0.59	-	0.11	0.06	-	0.11	0.38
	8	-	-	-	-	-	-	-	0.16	0.06	-	0.87	0.30
	9	-	-	-	-	-	-	-	0.17	0.23	-	0.97	0.37
	10	-	-	-	-	-	-	-	**0.05**	0.18	-	0.15	0.40
	11	-	-	-	-	-	-	-	**0.05**	0.59	-	0.15	0.91
	12	-	-	-	-	-	-	-	-	0.86	-	-	0.26

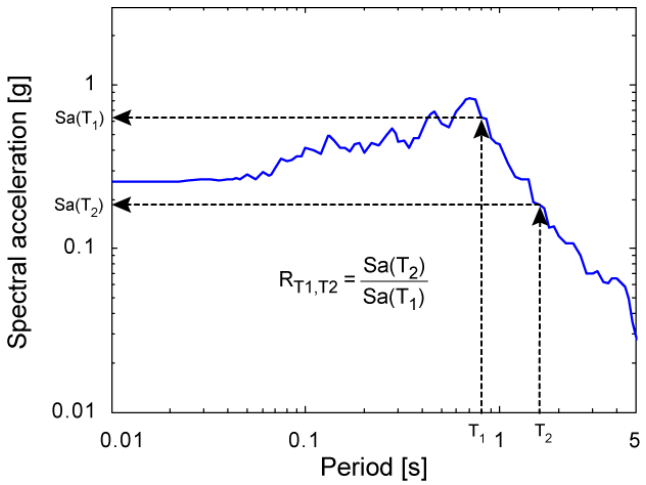

Figure 1: Calculation of $R_{T1,T2}$ for a given response spectrum.

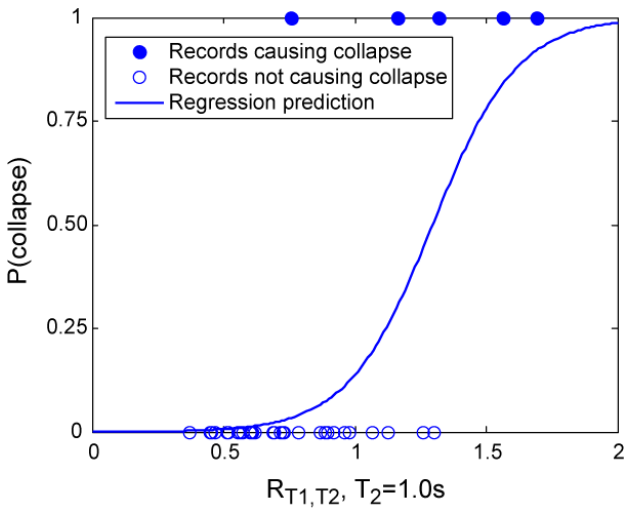

Figure 2: An example of prediction of the probability of collapse using logistic regression applied to binary collapse/non-collapse results ($Sa(T_1) = 0.9g$).

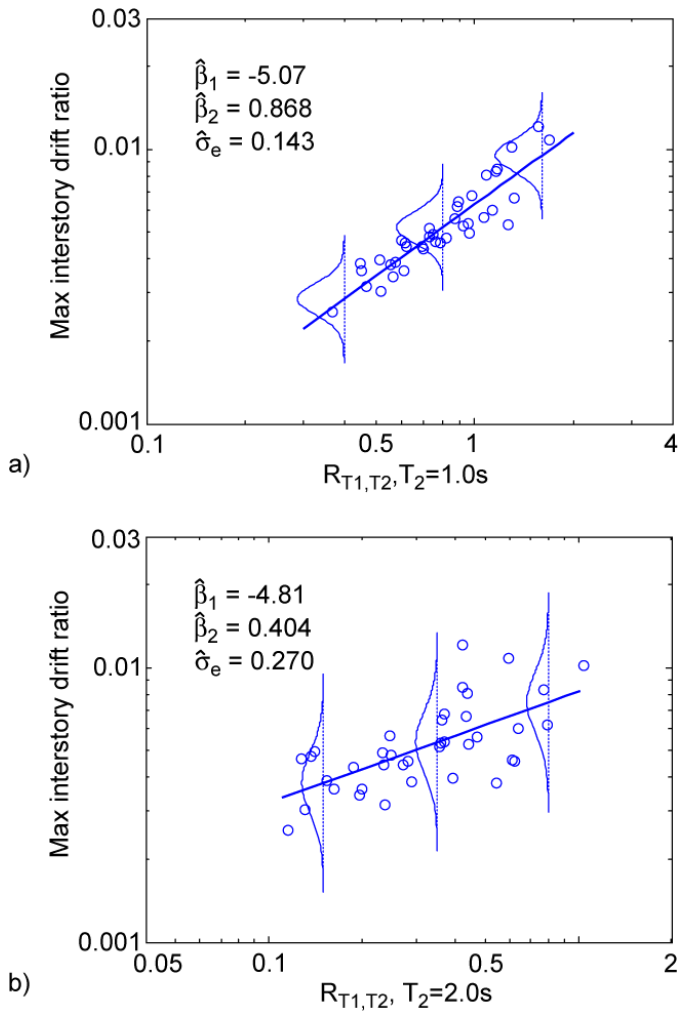

Figure 3: Comparison of the effectiveness of $R_{T1,T2}$ with two potential T_2 values, evaluated for response results from the primary structure of interest with records scaled to $Sa(T_1)$=0.3g. (a) a T_2 choice with high efficiency, and (b) a T_2 choice with low efficiency.

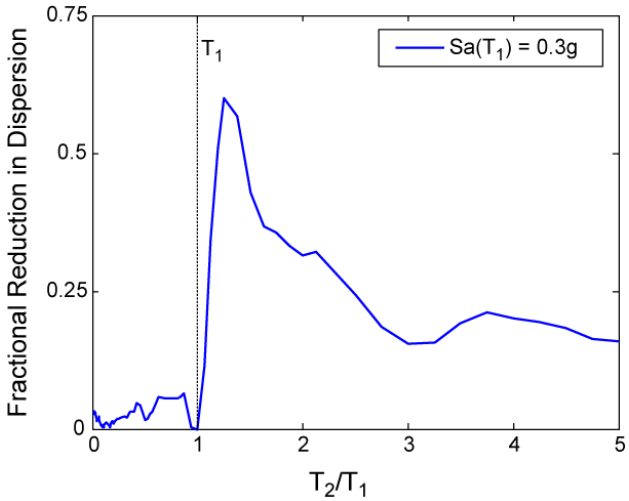

Figure 4: Fractional reduction in dispersion vs. T_2/T_1 for $Sa(T_1)$=0.3g.

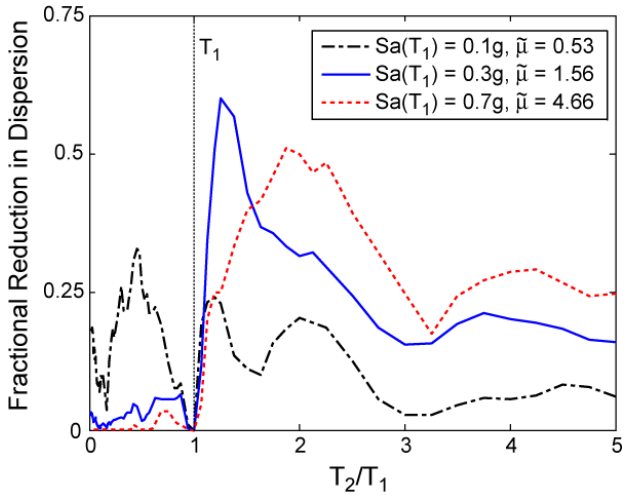

Figure 5: Fractional reduction in dispersion vs. T_2/T_1 for three levels of $Sa(T_1)$.

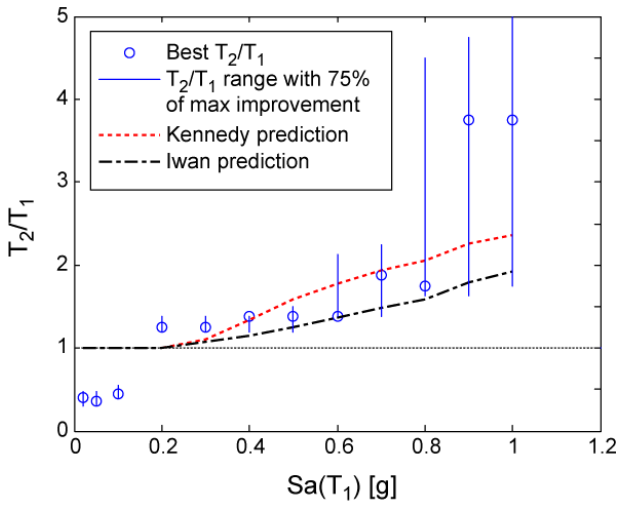

Figure 6: Optimal T_2/T_1 versus $Sa(T_1)$, compared periods for equivalent linear systems suggested by Kennedy [1985] and Iwan [1980].

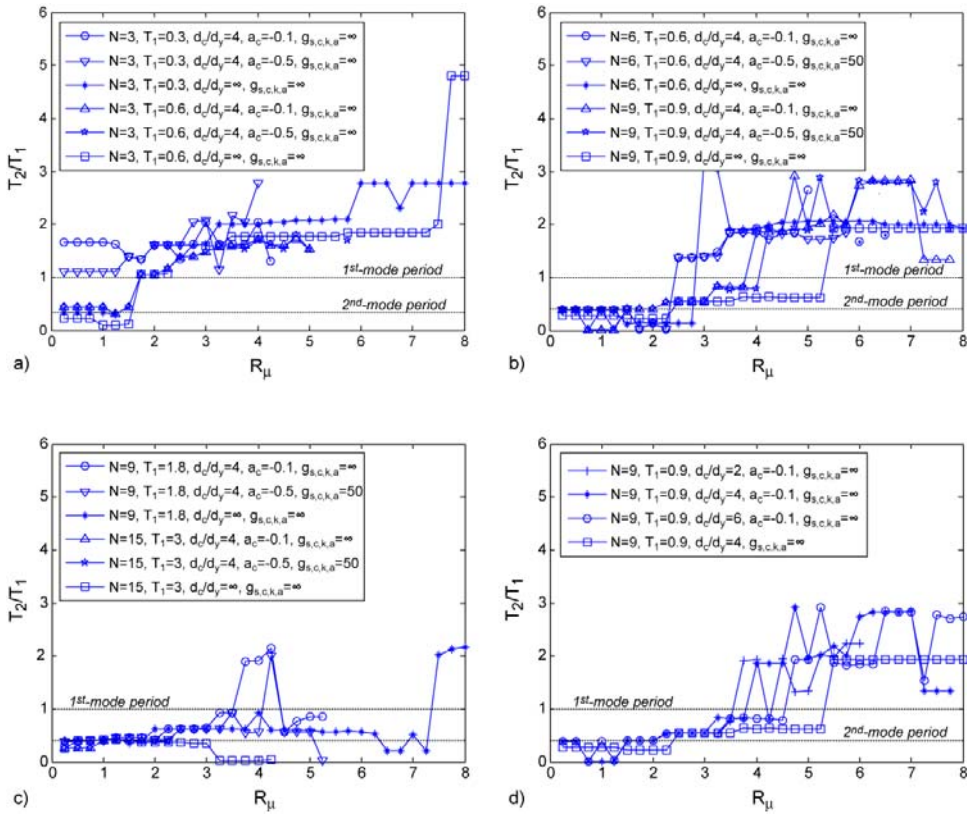

Figure 7: Optimal T_2/T_1 for four groups of structures: (a) three-story structures dominated by first-mode response, (b) six- and nine-story structures with moderate contribution from second-mode response, (c) nine- and fifteen-story structures with significant contribution from second-mode response, and (d) nine-story structures with varying levels of element ductility.

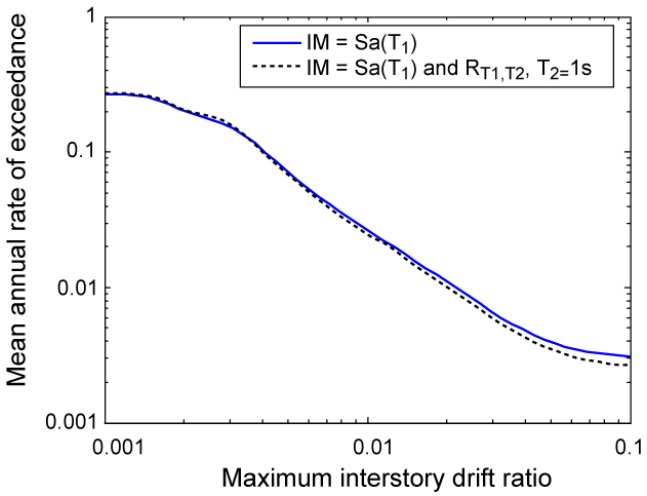

Figure 8: Maximum interstory drift hazard curves computed using the scalar *IM* $Sa(T_1)$ and a vector *IM* incorporating $Sa(T_1)$ $R_{T1,T2}$.

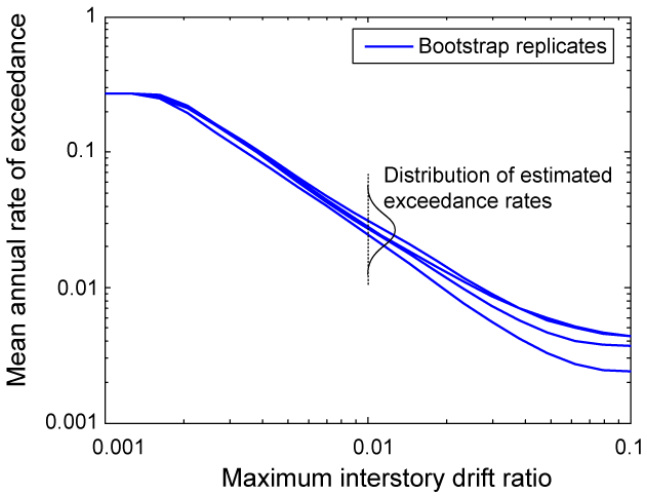

Figure 9: Example bootstrap replicates of the vector *IM* drift hazard curve, illustrating how the distribution of estimated exceedance rates is computed.

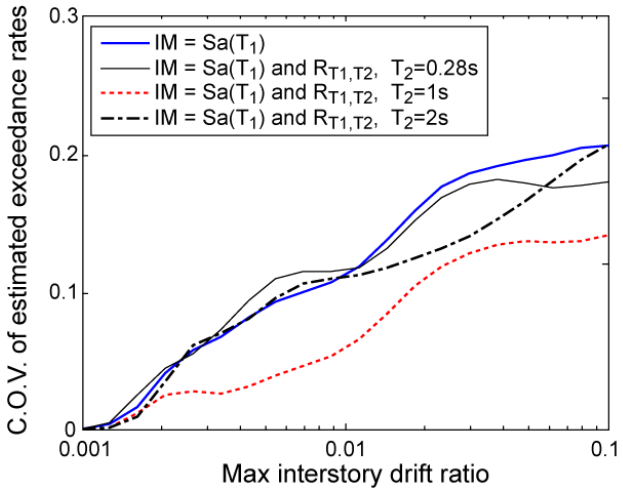

Figure 10: Coefficient of variation (C.O.V.) of estimated exceedance rates versus maximum interstory drift ratio with a scalar *IM* and three candidate vector *IM*s.

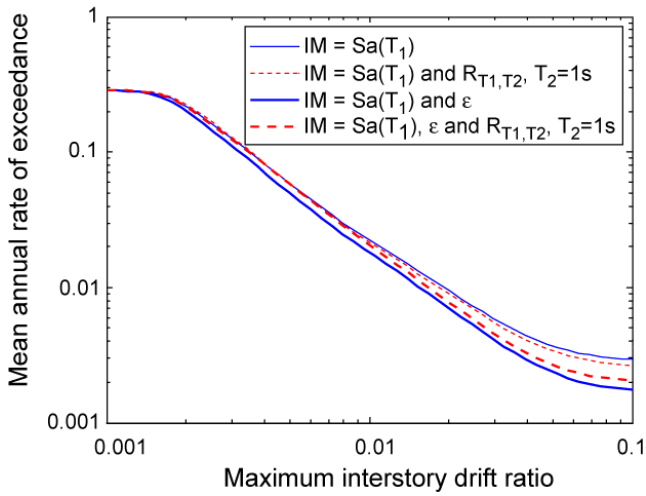

Figure 11: Maximum interstory drift hazard curves computed using the scalar *IM* $Sa(T_1)$ and vector *IM*s incorporating $Sa(T_1)$ and $R_{T1,T2}$, ε, or both.

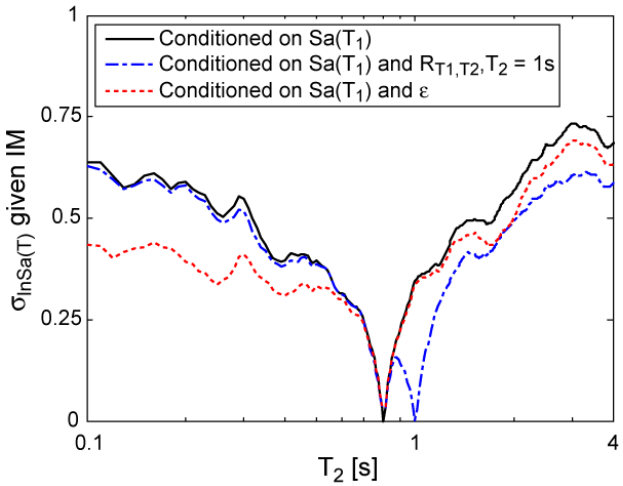

Figure 12: Conditional standard deviation of ln*Sa*(*T*) given *IM*, for three *IM*s.

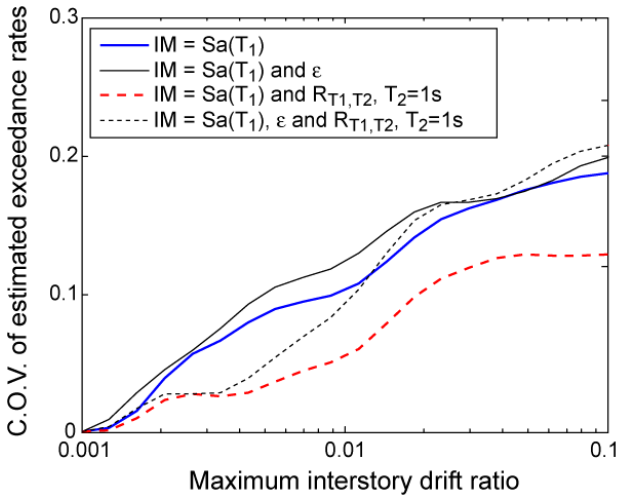

Figure 13: Coefficient of variation (C.O.V.) of estimated exceedance rates versus maximum interstory drift ratio for drift hazard curves computed using the scalar *IM* $Sa(T_1)$ and vector *IM*s incorporating $Sa(T_1)$ and $R_{T1,T2}$, ε, or both.